










Fruit setting rewires central metabolism via gibberellin cascades

Yoshihito Shinozaki^{a,b,c,1} , Bertrand P. Beauvoit^d , Masaru Takahara^a , Shuhei Hao^a, Kentaro Ezura^{a,b} , Marie-Hélène Andrieu^d, Keiji Nishida^e, Kazuki Morif^f, Yutaka Suzuki^g, Satoshi Kuhara^f, Hirofumi Enomoto^{h,i} , Miyako Kusano^{a,c,j}, Atsushi Fukushima^j , Tetsuya Mori^j, Mikiko Kojima^j, Makoto Kobayashi^j, Hitoshi Sakakibara^{j,k} , Kazuki Saito^{j,l}, Yuya Ohtani^a, Camille Bénard^d, Duyen Prodhomme^d, Yves Gibon^d, Hiroshi Ezura^{a,c} , and Tohru Ariizumi^{a,c,2} 

^aFaculty of Life and Environmental Sciences, University of Tsukuba, Tsukuba, Ibaraki 305-8572, Japan; ^bJapan Society for Promotion of Science, Kojimachi, Tokyo 102-0083, Japan; ^cTsukuba Plant Innovation Research Center, University of Tsukuba, Tsukuba, Ibaraki 305-8572, Japan; ^dUniv. Bordeaux, l'Institut National de Recherche en Agriculture, Alimentation et Environnement, Biologie du Fruit et Pathologie, UMR 1332, F-33140 Villenave d'Ornon, France; ^eEngineering Biology Research Center, Kobe University, Chuo-ku, Kobe, Hyogo 650-0047, Japan; ^fFaculty of Agriculture, Kyushu University, Fukuoka 819-0395, Japan; ^gDepartment of Computational Biology and Medical Sciences, Graduate School of Frontier Sciences, University of Tokyo, Kashiwa, Chiba 277-8561, Japan; ^hDepartment of Biosciences, Teikyo University, Utsunomiya, Tochigi 320-8551, Japan; ⁱAdvanced Instrumental Analysis Center, Teikyo University, Utsunomiya, Tochigi 320-8551, Japan; ^jRIKEN Center for Sustainable Resource Science, Yokohama, Kanagawa 230-0045, Japan; ^kGraduate School of Bioagricultural Sciences, Nagoya University, Nagoya, Aichi 464-8601, Japan; and ^lGraduate School and Faculty of Pharmaceutical Sciences, Chiba University, Chiba 260-8675, Japan

Edited by Zachary B. Lippman, Cold Spring Harbor Laboratory, Cold Spring Harbor, NY, and accepted by Editorial Board Member Joseph R. Ecker August 3, 2020 (received for review June 26, 2020)

Fruit set is the process whereby ovaries develop into fruits after pollination and fertilization. The process is induced by the phytohormone gibberellin (GA) in tomatoes, as determined by the constitutive GA response mutant *procera*. However, the role of GA on the metabolic behavior in fruit-setting ovaries remains largely unknown. This study explored the biochemical mechanisms of fruit set using a network analysis of integrated transcriptome, proteome, metabolome, and enzyme activity data. Our results revealed that fruit set involves the activation of central carbon metabolism, with increased hexoses, hexose phosphates, and downstream metabolites, including intermediates and derivatives of glycolysis, the tricarboxylic acid cycle, and associated organic and amino acids. The network analysis also identified the transcriptional hub gene *SIHB15A*, that coordinated metabolic activation. Furthermore, a kinetic model of sucrose metabolism predicted that the sucrose cycle had high activity levels in unpollinated ovaries, whereas it was shut down when sugars rapidly accumulated in vacuoles in fruit-setting ovaries, in a time-dependent manner via tonoplasmic sugar carriers. Moreover, fruit set at least partly required the activity of fructokinase, which may pull fructose out of the vacuole, and this could feed the downstream pathways. Collectively, our results indicate that GA cascades enhance sink capacities, by up-regulating central metabolic enzyme capacities at both transcriptional and posttranscriptional levels. This leads to increased sucrose uptake and carbon fluxes for the production of the constituents of biomass and energy that are essential for rapid ovary growth during the initiation of fruit set.

fruit set | gibberellin | metabolic enzymes | tomatoes | parthenocarpy

Fruit set marks the transition of ovaries into fruits and is generally induced by pollination and then fertilization. Pollination is usually essential for the induction of fruit set, as it stimulates the accumulation of plant growth regulators within fertilized ovaries, including plant hormones like auxin and gibberellin (GA). Gibberellins are tetracyclic diterpenoid hormones that stimulate aspects of plant development, such as root and shoot elongation, seed germination, flower transition, and fruit set and expansion (1). They stimulate these processes by disrupting proteins from the DELLA family of negative regulators (2, 3). The tomato genome contains a single copy of the DELLA homolog called PROCERA—and its loss-of-function mutant, *procera* (*pro*)—induces most of the GA responses; it has been consistently found that ~95% of the GA response genes in leaf

tissues are regulated by PROCERA (4, 5). However, the metabolic responses induced by GAs are poorly understood.

The roles of plant hormones are widely accepted in the regulation of fruit set initiation, especially auxin and GA, that act as positive regulatory signals triggering rapid ovary growth. Both auxin and GA are involved in the active cell division phase, whereas the cell expansion phase is dominated by GA in fruit-setting ovaries, and cell growth intensity is dependent on auxin and gibberellin dose and signaling (6). Furthermore, the exogenous application of these hormones onto ovaries or genetic mutations in the negative regulatory genes of these hormone cascades, such as *INDOLE-3 ACETIC ACID 9 (IAA9)* or *PROCERA*, can induce pollination-independent fruit set, termed parthenocarpy (7, 8). Although fruit set is induced by both auxin

Significance

Fruit set, which is triggered by the phytohormone gibberellin (GA), is the developmental transition of ovaries into fruits. Our multiomics approaches revealed that PROCERA-dependent GA responses rewired central carbon metabolism, predominantly under transcriptional control. The kinetic analysis approach used in this study enabled us to construct a carbon flux model of the earliest processes that occur during fruit set. The model revealed that fruit set coincided with the temporal changes in sugar compartmentalization due to the coordinated actions of the enzymes and tonoplasmic carriers and highlighted that fructokinase likely contributed to early ovary growth by pulling fructose out of the vacuole to feed the downstream pathways for biosynthesis of cell wall components and energy provision.

Author contributions: T.A. designed research; Y. Shinozaki, B.P.B., M.T., S.H., K.E., M.-H.A., K.N., Y. Suzuki, H. Enomoto, M. Kusano, T.M., M. Kojima, M. Kobayashi, Y.O., C.B., D.P., and T.A. performed research; Y. Shinozaki, B.P.B., K.M., S.K., A.F., H.S., K.S., Y.G., and T.A. analyzed data; and Y. Shinozaki, B.P.B., Y.G., H. Ezura, and T.A. wrote the paper.

The authors declare no competing interest.

This article is a PNAS Direct Submission. Z.B.L. is a guest editor invited by the Editorial Board.

Published under the PNAS license.

¹Present address: Institute of Global Innovation Research, Tokyo University of Agriculture and Technology, Fuchu, Tokyo 183-8509, Japan.

²To whom correspondence may be addressed. Email: ariizumi.toru.ge@u.tsukuba.ac.jp.

This article contains supporting information online at <https://www.pnas.org/lookup/suppl/doi:10.1073/pnas.2011859117/-DCSupplemental>.

First published September 3, 2020.

and GA, it generally requires GA biosynthesis or its signaling cascades; thus GA most likely acts downstream of auxin-mediated signaling during fruit set (9, 10). To decipher fruit set mechanisms, extensive transcriptome studies have been conducted using young ovaries to shed light on their molecular pathways. The main findings from these studies are highlighted by changes in mRNA transcripts associated with, for example, hormone metabolism and signaling, specific families of transcription factors (TFs) (for instance, MADS box and homeobox), photosynthesis, cell division and expansion, and the metabolism of cell walls and carbohydrates (11, 12). However, how these transcriptome fluctuations affect metabolic pathways, particularly the sugar and central metabolism pathways, is poorly understood. Their associations have been implicated with genetic evidence that the silencing of sucrose (Suc) cleavage genes, such as *SUCROSE SYNTHASE 1* (*SuSy1*) or *LYCOPERSICON INVERTASE5* (*LIN5*), results in reduced fruit set efficiency, as well as the fact that the down-regulation of *IAA9*, encoding a negative regulatory protein of auxin responses, induces parthenocarpic associated with the accumulation of high levels of the major sugars and hexose phosphates in fruit-growing ovaries (12–14). Additionally, organic compound polyamines in ovaries have been shown to play important roles in early ovary growth, as growth regulators or nitrogen sources (15). These results have led to speculation about whether activated sugar and carbohydrate metabolism and subsequent downstream metabolic pathways were critical for fruit set initiation, but current biochemical evidence is limited.

Systems biology approaches have been widely applied to decipher the fundamental mechanisms of fruit development and ripening in tomato, by assessing their transcripts, proteins, metabolites, and enzymes (16–18). These analyses have identified subsets of components that specifically fluctuate during fruit development and ripening. Furthermore, kinetic modeling analysis, integrating both tonoplastic carriers and sugar metabolizing enzymes, has revealed the tight correlations between sugar uptake and vacuolar expansion and enabled the precise prediction of metabolic behaviors (19). However, the earliest stages of fruit development, including fruit set initiation, have yet to be investigated with this systematic approach. To address this, multiomics approaches were carried out and comprehensive distributions of the molecular and metabolic components were determined. A kinetic model to calculate sugar fluxes and partitioning in young fruit-setting ovaries was also constructed. Our results shed light on the currently unknown role of GAs in rewiring the metabolic status of ovaries for high carbohydrate metabolizing activities. These activities allow for active metabolic fluxes and the generation of energy and components that are essential for rapid ovary growth.

Results

Comparison of Ovary Growth in Wild Type and *pro* during Fruit Set.

Ovary growth for the wild-type (WT) tomato and the *procera* mutant (*pro*) during fruit set, in the defined conditions of this investigation, was assessed. The ovary weight and histology of the ovary wall were nearly equivalent for the WT and *pro*, both –2 and 0 d after anthesis (DAA) (Fig. 1 A–C and *SI Appendix, Fig. S1*). The weight of the WT ovaries increased greatly with pollination 4 DAA, with a 100% fruit set rate, unlike the nongrowing unpollinated WT ovaries that showed little change. In contrast, the unpollinated *pro* ovaries had an 81% pollination-independent fruit set rate, through parthenocarpic; hand pollination increased this to 100%, and there were concomitant increases in ovary weight by 4 DAA. Fruit-growing ovaries (pollinated WT or both pollinated and unpollinated *pro* ovaries) showed drastic increases in the cell layers and size, due to intense cell division and strong cell expansion, respectively, between

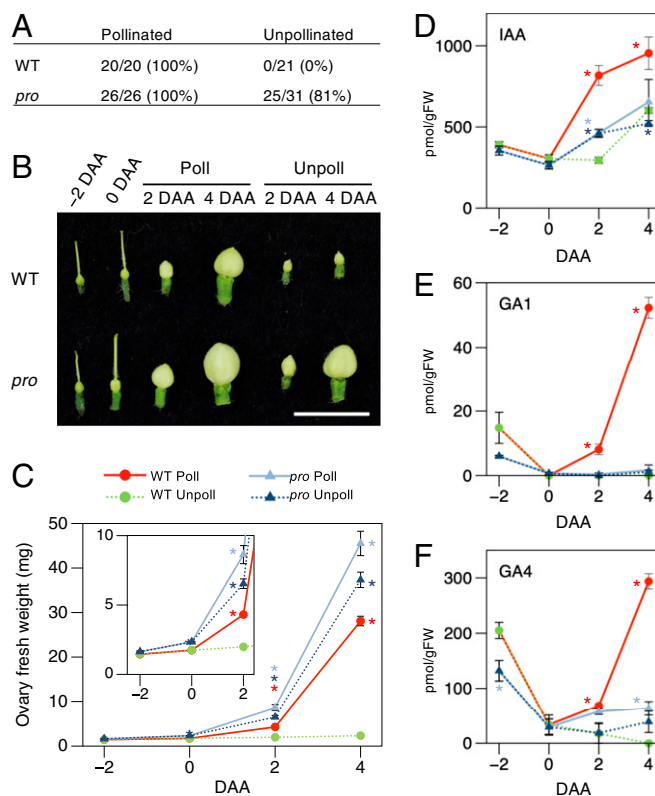


Fig. 1. Fruit set in WT tomato and the GA response mutant *procera* (*pro*). (A) Pollination- and parthenocarpic-dependent fruit set rate. Number of developed fruits per attempt is also shown. (B and C) Representative pictures (B) and weights (C) of pollinated and unpollinated ovaries from –2 to 2 DAA (Inset) or 4 DAA. Values in C are mean \pm SEs of six replicates, each one defined as the average ovary weight obtained by measuring a mixture of 5 to 10 ovaries. (D–F) Endogenous levels of IAA (D) and bioactive GAs (E and F). Values in D–F are mean \pm SEs of three replicates. (Scale bar in B, 1 cm.) Asterisks in C–F indicate significant differences from nongrowing unpollinated WT ovaries (Student's *t* test, $P < 0.05$). DAA, days after anthesis; Poll, pollination; Unpoll, unpollinated.

0 and 4 DAA (*SI Appendix, Fig. S1*). In the pollinated WT ovaries, cell division that commenced by 2 DAA resulted in a slight increase in ovary weight, whereas cell enlargement likely contributed to a rapid increase in ovary weight between 2 and 4 DAA. Unpollinated *pro* ovaries showed similar cell division activity, but their cell enlargement was more prominent than the pollinated WT. Pollination of the *pro* further activated cell proliferation 2 DAA, which contributed to thicker ovary walls.

Changes in Hormonal Dynamics during Fruit Set. Hormonal dynamics in the ovaries, coupled with the associated hormone transcript profiles, were investigated. In contrast to nongrowing unpollinated WT ovaries, the levels of auxin (indole acetic acid or IAA) in the pollinated ovaries rapidly increased 2 DAA and persisted until 4 DAA. While the levels of bioactive GAs (GA_1 and GA_4) were also stimulated by pollination 2 DAA, a notable increase was observed between 2 and 4 DAA (Fig. 1 D–F). The levels of auxin and bioactive GAs agreed with active cell division persisting until 4 DAA, and the notable cell expansion between 2 and 4 DAA. Transcriptome profiling by RNA sequencing (RNA-Seq) analysis revealed that in the fruit-growing WT ovaries, the hormone levels correlated with the transcripts of their key metabolism genes—i.e., *TAR1*, *toFZY2*, and *toFZY5* for auxin, and *SIGA20ox1* and *SIGA20ox2* for GA (20) (*SI Appendix,*

Fig. S2 and Dataset S1). In contrast, the levels of bioactive GAs in the *pro* ovaries were always lower than in the WT, indicating negative feedback regulations in their biosynthetic genes due to the constitutive GA response (21) (Fig. 1 E and F and *SI Appendix*, Fig. S2B). Both the pollinated and unpollinated *pro* ovaries accumulated lower amounts of auxin and transcripts encoding auxin biosynthesis genes than in the pollinated WT (Fig. 1D and *SI Appendix*, Fig. S2A), suggesting that the GA response counteracts auxin biosynthesis in the tomato ovary. Nevertheless, the *pro* ovaries showed auxin-dependent responses for some auxin signaling genes, such as the down-regulation of *ARF5* and *ARF7*, which were also suppressed in the pollinated WT ovaries (*SI Appendix*, Fig. S2A) and are known to act as repressors of fruit set initiation (9, 22, 23). Unpollinated *pro* ovary growth through parthenocarpy is thus unlikely to be related to the absolute levels of those hormones, but rather associated with the constitutive GA responses underlying the GA-regulatory PROCERA network, in which there is some auxin signaling cascade cross-talk.

Transcript and Metabolite Profiling and Integrated Network Analysis of Fruit Set. Besides RNA-Seq, metabolomic analysis by gas chromatography-time-of-flight-mass spectrometry (GC-TOF-MS) and high-performance liquid chromatography coupled with photodiode array detector (LC-PDA) analyses were performed to examine and compare the dynamics of the transcript and metabolite profiles during fruit setting. The GC-TOF-MS analysis systematically detected 252 metabolites as unique peaks, and the LC-PDA analysis quantified six major hydrophobic pigments including carotenoids and chlorophylls (Dataset S2). A principal component analysis (PCA) revealed that the transcriptomes and metabolomes clearly discriminated between fruit-growing and nongrowing ovaries (*SI Appendix*, Fig. S3). Profiles obtained for the WT and *pro* were strongly correlated -2 DAA, but less so after anthesis. However, both the transcript and metabolite profiles in the fruit-growing ovaries had clear clusters corresponding to each time point, indicating that these ovaries largely share transcript and metabolite profiles, and therefore parthenocarpy can mimic pollination-dependent molecular and biochemical mechanisms.

To reveal the biochemical and regulatory networks of fruit set, we applied a weighted gene coexpression network analysis (WGCNA) using 12,322 transcripts that showed a high variation among sample types and 101 identified or provisionally identified metabolites from the GC-TOF-MS and LC-PDA analyses (*SI Appendix*, *Materials and Methods* and Datasets S3 and S4). This analysis is based on pairwise correlations between the levels of each transcript or metabolite and it identified a total of 31 transcriptional gene expression modules (GenM1 to GenM31) and seven metabolite modules (MetM1 to MetM7) (Fig. 2 A and B and Datasets S3 and S4). The module eigengene (MEgene) and eigenmetabolite (MEMetabolite) values, which are considered the first principal components of the profiles in the individual modules (24), summarized the accumulation patterns of the clustered transcripts and metabolites and the intermodular similarities (Fig. 2 A and B and *SI Appendix*, Figs. S4 and S5). Several significant correlations appeared to be present in the module correlation map (Pearson correlation coefficient [PCC] > 0.75 , $P < 0.05$; Fig. 2C). The highest correlation between transcript-metabolite modules was found between GenM3 and MetM1 (PCC = 0.943), and while GenM3 also showed a significant correlation with MetM2 (PCC = 0.806), together with the GenM2–MetM1 module correlation (PCC = 0.811), these created a subnetwork (SN-1) associated with high levels of transcripts and metabolites after anthesis, which were maintained until 4 DAA in the fruit-growing ovaries. We also

found significant correlations between MetM3 and GenM7 (PCC = 0.850) and GenM2 (PCC = 0.856), which created another subnetwork (SN-2) associated with early responses 2 DAA in the fruit-growing ovaries. SN-1 and SN-2 were part of a fruit-growing transcript-metabolite network with the significantly connected GenM2 and MetM1 (PCC = 0.811) as the inter-subnetwork hubs (Fig. 3). When focused on transcriptome correlation, both GenM2 and GenM3 showed strong negative correlations with the largest transcript module GenM1 (PCC = -0.943 and -0.867 , respectively), which showed a clear negative association with fruit-growing ovaries (Fig. 2 A and C).

To determine the functional associations of the module networks, we constructed an interconnection map for the transcript modules with the gene ontology (GO) terms that exhibited the lowest P values (Fig. 3 and Dataset S5). GenM2 and GenM3 were found to enrich the GO terms related to carbohydrate metabolism and/or energy production, such as “carbohydrate metabolic process,” “glycolytic process,” “xyloglucan metabolic process,” “cell wall organization,” and “ATP synthesis coupled protein transport” (Dataset S5), and these correlated to form metabolite modules MetM1 to 3, that included major intermediates and derivatives of the carbohydrate and sugar metabolism (Fig. 3). The metabolites enriched in the MetM3 module showed strong increases 2 DAA in the fruit-growing ovaries, especially fructose-6-phosphate (F6P) and glucose-6-phosphate (G6P), which are involved in glycolysis and Suc and starch metabolism. The MetM3 module also contained the polyamine spermidine that promotes fruit set through the modulation of GA metabolism in tomato (15). The MetM2 module included fructose (Fru) and glucose (Glc) as well as derivatives and intermediates of the gamma-aminobutyric acid (GABA) biosynthetic pathway that partially bypasses the tricarboxylic acid cycle (TCA) cycle, including 5-oxoproline (pyroglutamate), ornithine, and glutamine, as well as four amino acids (alanine, serine, threonine, and glutamine). The MetM2 module also contained shikimic acid, which originates from phosphoenolpyruvate (glycolysis) and erythrose-4-phosphate (oxidative/reductive pentose phosphate pathway) and is the precursor of aromatic amino acids and phenylpropanoids, which are used to generate pigments, hormones, and cell wall components including lignin (25). These data indicate that both central carbon and nitrogen metabolism are rapidly activated in fruit-growing ovaries. The MetM1 module, which peaked 4 DAA (*SI Appendix*, Fig. S5), included seven amino acids and three organic acids (citric acid, malic acid, and fumaric acid), which are intermediates of the TCA cycle and vacuolar storage compounds, and therefore play an important role in the energy and osmotic status of pericarp cells (26). These data also suggested a continuous activation of the central metabolism between 0 and 4 DAA. Matrix-assisted laser desorption ionization mass spectrometry imaging (MALDI-MSI) analysis confirmed that some of the major metabolites described above, including hexoses ($m/z = 179.1$, $[M-H]^-$), GABA ($m/z = 102.1$, $[M-H]^-$), citric acid/isocitric acid ($m/z = 191.1$, $[M-H]^-$), malic acid ($m/z = 133.0$, $[M-H]^-$), and fumaric acid ($m/z = 115.0$, $[M-H]^-$), accumulated in rapidly growing maternal tissues, such as the pericarp and placenta, in growing ovaries 4 DAA, rather than the ovules, regardless of whether the pollination/fertilization was dependent or independent of fruit set (*SI Appendix*, Fig. S6). Taken together, transcriptomes associated with central metabolism pathways, spanning sugar and carbohydrate metabolism, glycolysis, and the TCA cycle, were correlated with their corresponding metabolomes that could have a major biochemical impact on the expansive growth of the ovary during fruit set initiation.

In contrast to those metabolite modules, the MetM6 module showed a clear negative association with the fruit-growing

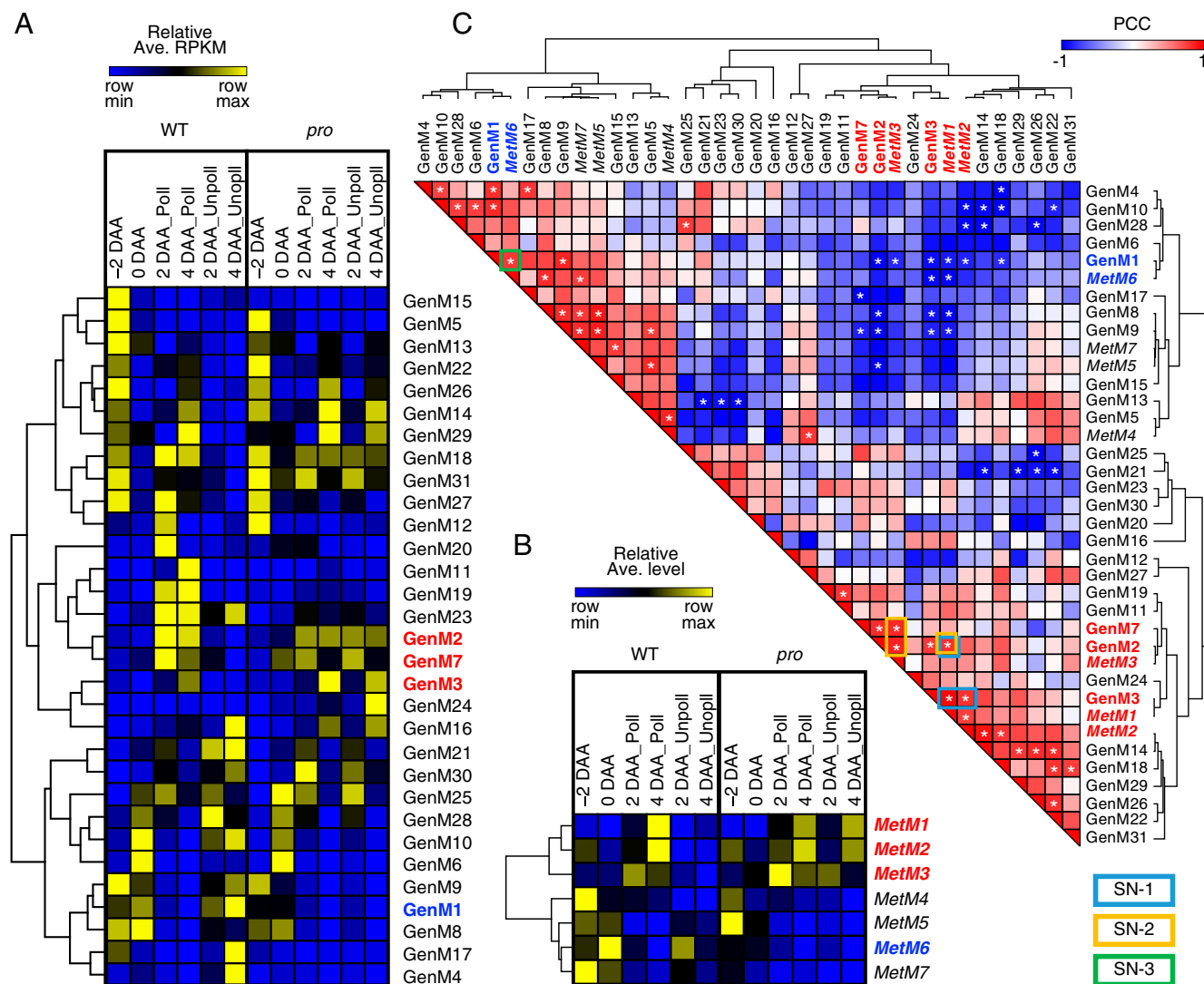


Fig. 2. Network analysis across pollinated and unpollinated ovaries in WT tomato and *procera* (*pro*) mutants. (A and B) Heat map showing averaged relative reads per kilobase of the exons per million mapped reads (RPKM) of genes (A) and relative levels of metabolites (B) clustered in the individual WGCNA gene transcript (GenM) and metabolite (MetM) modules. (C) PCC of each pair of GenM and MetM module. Asterisks indicate pairs with PCC > 0.75 or < -0.75 ($P < 0.05$). Fruit set associated GenM–MetM subnetworks are indicated by blue (SN-1), orange (SN-2), or green (SN-3) boxes, which correspond to positive associations with fruit set until 4 DAA, 2 DAA, and a negative association with fruit set, respectively. Among the modules consisting of these subnetworks, those positively and negatively associated with fruit set are indicated by bold red and blue, respectively. Metabolite modules are indicated by italic. DAA, days after anthesis; Poll, pollinated; Unpoll, unpollinated.

ovaries, and included metabolites known to be accumulated in senescing organs such as serotonin, raffinose, and alpha-tocopherol (27–29). Thus, GA signaling reduced the level of senescence-related metabolites, thereby suppressing the progression of ovary senescence. The GenM1 module, that was positively correlated with MetM6 (PCC = 0.779), enriched senescence-related GO terms such as “ethylene-activated signaling pathway” and “autophagy,” and these created a subnetwork (SN-3) negatively associated with fruit set (Figs. 2C and 3). This agreed with the notion that ethylene signaling and ovary senescence counteracted fruit set initiation (30, 31).

Functional Analysis of a Transcriptional Hub Negatively Associated with Fruit Set. Interestingly, GenM1, the largest transcript module, showed a negative association with fruit set, which suggested a potential importance for negative functional networks in fruit set (Fig. 2 and *SI Appendix*, Fig. S4). The fact that the inverse

correlation of GenM1 with the modules that were positively associated with fruit set, including the next largest transcript modules GenM2 (PCC = -0.943) and GenM3 (PCC = -0.867), as well as metabolite modules MetM1 (PCC = -0.830), MetM2 (PCC = -0.802), and MetM3 (PCC = -0.782), suggested that GenM1 was a hub module of the fruit set network (Figs. 2C and 3). TFs potentially play important roles in the regulation of transcriptional networks. We found that there were five families that accounted for over 25% of the TF members in the GenM1 module (Fig. 4A). Among the members of these families, a class III homeodomain-leucine zipper gene (Soylc03g120910)—a homolog of the *Arabidopsis* *CORONA* (*CNA*)—that is known to be associated with carpel cell development (32) was identified as a central hub gene (module membership [kME] = 0.922; *Dataset S3*), and its homologous gene in tomatoes is called *Solanum lycopersicum* *HOMEBOX 15A* (*SIHB15A*) (33). To examine the function of *SIHB15A* in fruit set, we generated putative knockout

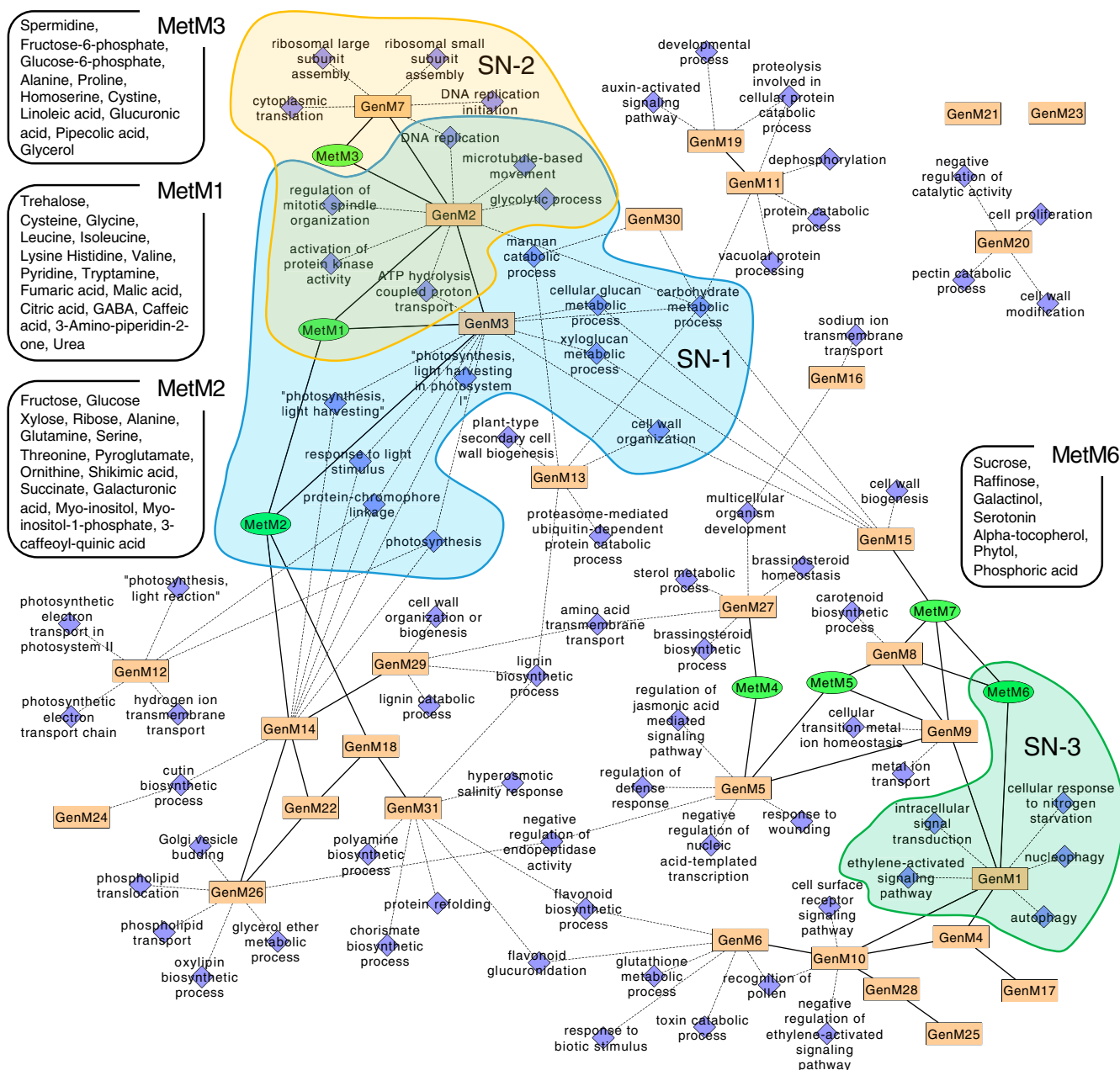


Fig. 3. Integrated network of transcript and metabolite modules. The orange rectangles and green circles represent nodes of coexpression of the WGCNA transcript (GenM) and metabolite (MetM) modules, respectively. Blue squares connected by dashed lines to transcript modules represent the nodes from the top five GO terms enriched in each module (false discovery rate [FDR]-adjusted P value < 0.05 , hypergeometric test). Edges with solid lines represent inter-modular correlation ($PCC > 0.75$, $P < 0.05$). The identified metabolites included in fruit set-associated modules with $kME > 0.7$ are shown. Fruit set-associated GenM–MetM subnetworks (SN-1, -2, and -3; Fig. 2C) and the metabolites included in the subnetworks are also shown.

plants by incorporating the stop codon within the first exon, using a modified CRISPR-Cas9 system that allowed for single base substitutions (34) and confirmed that the genome edit resulted in a homozygous mutation devoid of T-DNA integration (Fig. 4B). The putative *SIHB15A*-knockout (*Slhb15a-ko*) plants showed efficient parthenocarpy, with similar cytology to *pro*-induced parthenocarpy, in that active cell enlargement rather than cell division, largely contributed to rapid ovary growth (Fig. 4C–H and SI Appendix, Fig. S1). Moreover, the parthenocarpic ovary transcriptome was obtained by RNA-Seq. At 4 DAA, the *Slhb15a-ko* was highly similar to that of the pollinated WT (Fig. 4I, SI Appendix, Materials and Methods, and Dataset

S6) and parthenocarpic *pro* (Fig. 4J). Furthermore, a high similarity of the transcripts of the 92 selected genes associated with the central metabolism (SI Appendix, Fig. S7) was observed between the transcriptome of parthenocarpic *Slhb15a-ko* and that of the pollinated WT (Fig. 4K) and parthenocarpic *pro* (Fig. 4L). Thus, our results demonstrated that the network construction analysis makes it possible to identify key gene hubs. *SIHB15A* likely coordinates the regulation of central metabolism pathways by PROCERA in fruit set.

Correlations between Transcripts and Proteins during Fruit Set. We analyzed the proteome using label-free shotgun proteomics with

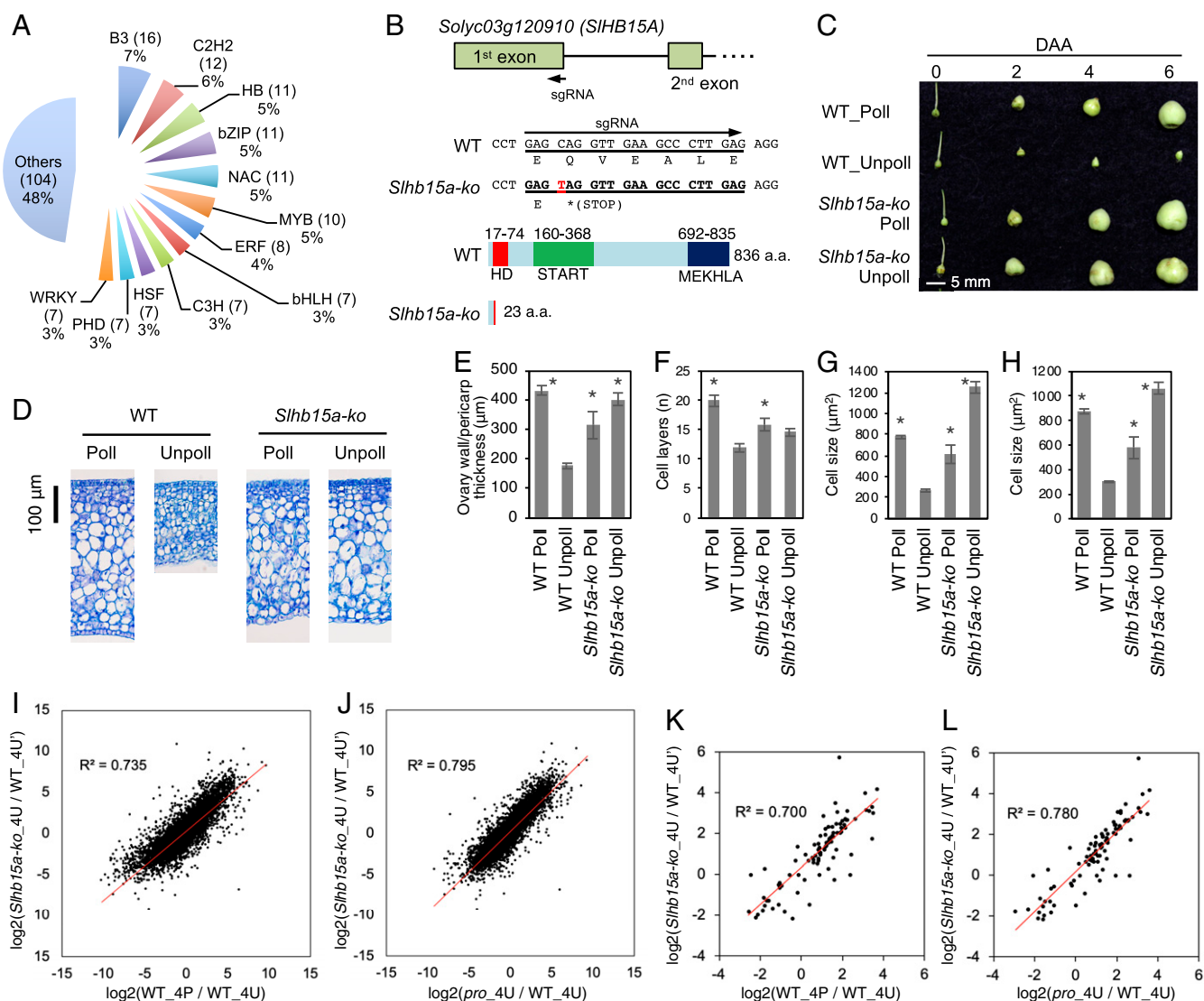


Fig. 4. Targeted mutagenesis of the homolog of *Arabidopsis* *CNA* and its effect on ovary growth and transcriptome. (A) The family of transcription factors that are included in the GenM1 module. (B) Target sites specified by sgRNA and the edited genome and amino acid sequences in the putative knockout plant (*Slhb15a-ko*)—with a stop codon at the 24th amino acid altered using the modified CRISPR-Cas9 system (target-activation induced cytidine deaminase [Target-AID]). The three functional domains (homeodomain [HD], START, and MEKHLA), their positions on the SIHB15A protein, and the putative truncated protein structure in *Slhb15a-ko* are shown. (C) Parthenocarpy exhibited in *Slhb15a-ko*. (D) Representative sections of the ovary walls 4 DAA for Poll and Unpoll. (E–H) The thickness (E), number of cell layers (F), and mean cell size of internal (G) and external (H) mesocarp in the ovary wall 4 DAA. Values are means \pm SEs of three independent ovaries. Asterisks in E–H indicate significant differences from nongrowing unpollinated WT ovaries (Student's *t* test, $P < 0.05$). (I–L) Transcript correlations between parthenocarpic *Slhb15a-ko* ovaries and pollinated WT ovaries (I and K) or parthenocarpic *pro* ovaries 4 DAA (J and L). Scatterplots show the \log_2 fold changes of 18,775 commonly expressed genes (I and J) or 92 selected genes associated with central metabolism shown in SI Appendix, Fig. S7 (K and L) between unpollinated WT ovaries and pollinated WT, unpollinated *Slhb15a-ko*, or unpollinated *pro* ovaries. WT_4U and WT_4U' indicate different batches of unpollinated WT ovaries analyzed together with pollinated WT and unpollinated *pro* ovaries (unpollinated *Slhb15a-ko*, respectively. DAA, days after anthesis; 4P, 4 DAA with pollination; 4U (4U'), 4 DAA without pollination; Poll, pollination; Unpoll, unpollinated.

the ovaries depicted in Fig. 1B. A total of 1,343 proteins were systematically detected from three replicates of each ovary sample derived from pollinated or unpollinated WT and unpollinated *pro* plants (Dataset S7). A PCA assessed the similarities of the protein profiles and revealed the clusters of proteins associated with the ovary growth stages. The results were similar to those of the transcripts and metabolites, as the fruit-growing ovaries were closely related and were discriminated from the unpollinated WT ovaries (SI Appendix, Fig. S8).

Abundance correlations between the transcripts and proteins were significantly positive for all sample types (SI Appendix, Table S1). Correlations between the individual transcripts and

the corresponding proteins were determined and compared across different MapMan functional categories (35) (SI Appendix, Fig. S9). Overall, positive correlations were observed, except for the transport-related proteins. High correlations during both pollination-dependent and pollination-independent fruit set were observed among several functional categories that were related to central metabolism, such as “carbohydrate metabolism,” “glycolysis/gluconeogenesis,” “TCA cycle and mitochondrial electron transfer chain,” “cell wall,” and “nitrogen and amino acid metabolism.” This suggests that the reprogramming of central metabolism that occurs during early fruit growth is in large part under the control of transcription.

Integration of Metabolic Data into an Enzyme-Based Model of Fruit Setting. The activities of 36 enzymes across the central metabolism during fruit set were quantitatively measured (*SI Appendix, Fig. S10*). In total, 18 showed higher activity in the fruit-growing ovaries when compared with unpollinated WT ovaries 4 DAA (Student's *t* test, $P < 0.05$), indicating that fruit set eventually impacted the activities of many enzymes across central metabolism. Moreover, we identified genes whose transcript abundances were correlated with the corresponding protein abundances in the central metabolism pathways (*SI Appendix, Fig. S7*). For instance, transcript abundances of the fructokinase (FK; *FRK1* and *FRK2*), ADP glucose pyrophosphorylase (AGPase) small subunit 1 (*AGPS1*), fructose-6-phosphate 1-phosphotransferase (PFK; two *PFK* family members), fructose-bisphosphate (FBP)-aldolase (*FBA7* and *FBA8*), glyceraldehyde-3-phosphate dehydrogenase (GAPDH; *GAPC2*), enolase (*PGH1*), and malic enzyme (ME; two *ME* family members), were significantly associated with their corresponding protein abundances ($0.805 < \text{Spearman correlation coefficient [SCC]} < 0.874$; $P < 0.05$). Significant correlations were also found between the protein abundances and enzyme activities in *FRK1*, *FRK2*, *AGPS1*, *FBA7*, *FBA8*, and an *ME* family member ($0.762 < \text{SCC} < 0.881$;

$P < 0.05$; *SI Appendix, Table S2*). These results reinforce the idea that these pathways are strongly transcriptionally controlled during fruit set.

A kinetic model of sugar metabolism was constructed by integrating enzyme activity, subcellular compartmentation, and growth data, in which the carbon supply relied on a symplastic phloem unloading Suc (19, 36). We also integrated the absolute levels of seven major metabolites that were measured (*SI Appendix, Fig. S11A*). The parameterization of the core model was specific to each line (WT and *pro*), to each condition (with or without pollination), and to each time point (0, 2, and 4 DAA) (Fig. 1C and *SI Appendix, Table S3*). To optimize the model, we parameterized five unknown parameters (e.g., the Suc uptake flux [the capacity of the ovaries to import Suc] and the capacity of the tonoplastic sugar carriers) that were not experimentally obtained. The optimization process allowed us to determine the best values for these unknown parameters and allowed for the simulations to match the measurements (*SI Appendix, Fig. S12 and Table S4*). We found a parameter setting that enabled a good fit for the Suc, Glc, and Fru contents, the Suc-to-hexoses and Glc-to-Fru ratios (*SI Appendix, Fig. S13*), and, to some

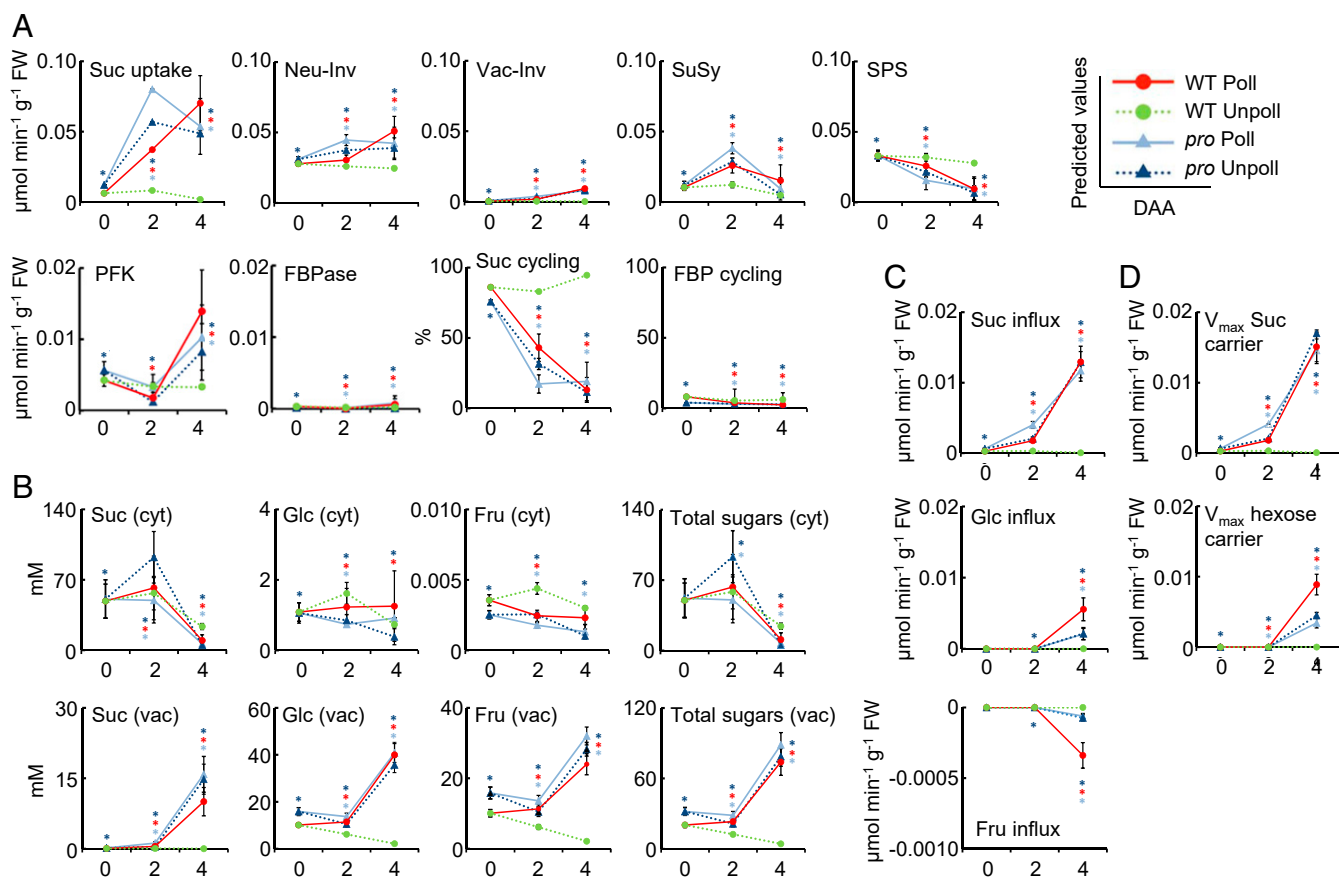


Fig. 5. Modeling of sugar metabolism in WT tomato and *procerca* (*pro*) mutant ovaries during fruit set. Models were parameterized according to the data in *SI Appendix, Table S3* and further optimized to fit the experimental data. (A) Fluxes of Suc uptake and Suc interconverting enzymes, expressed in $\mu\text{mol min}^{-1} \text{g}^{-1} \text{FW}$. The percentage of Suc cycling within the cytosol was calculated from the ratio between Suc synthesis and cleavage. The percentage of FBP cycling was calculated from the ratio between synthesis and hydrolysis. (B) Concentrations of each sugar within the cytosol (cyt) and the vacuole (vac), expressed in mM. The total sugar concentrations (Fru + Glc + Suc) in each compartment (cyt and vac) are also shown. (C and D) Sugar transport fluxes across the tonoplast (C) and transport capacities (V_{max}) of the Suc and hexose carriers (D), expressed in $\mu\text{mol min}^{-1} \text{g}^{-1} \text{FW}$. The x axis represents DAA. Data are means \pm SDs of the 200 best fits. Asterisks indicate significant differences from Student's *t* tests ($P < 0.05$) between the WT and *pro* ovaries 0 DAA, and between unpollinated WT (dotted light green line) and fruit-growing ovaries (pollinated WT [continuous red line], unpollinated *pro* [dotted blue line], and pollinated *pro* [continuous sky-blue line]) ovaries 2 and 4 DAA. Neu-Inv, neutral invertase; Vac-Inv, vacuolar acid invertase; SuSy, sucrose synthase; SPS, sucrose-phosphate synthase; PFK, ATP phosphofructokinase; FBPase, fructose 1,6-bisphosphatase; Fru, fructose; Glc, glucose; Suc, sucrose; FBP, fructose 1,6-bisphosphate.

extent, the content of sugar phosphates (*SI Appendix, Fig. S14*). The effects of unknown parameters on the modeling results were determined by calculating their sensitivity coefficients, that showed how the model variables (fluxes and concentrations) were sensitive to parameterization. Among the five unknown parameters, the Suc uptake flux showed the highest coefficient, suggesting that it was the most important factor for model fitness, regardless of the genotype (*SI Appendix, Fig. S15*). The model was then cross-validated using a different dataset obtained from WT ovaries 4 DAA, both with and without pollination (*SI Appendix, Table S5*). Using this dataset and the five unknown parameters optimized with the first dataset (*SI Appendix, Table S4*), we found a reasonable consistency between the measured and simulated sugar contents with a linear correlation ($P = 0.0097$; *SI Appendix, Fig. S16A*). This correlation was further improved by optimizing the value of the Suc uptake flux ($P = 0.0068$; *SI Appendix, Fig. S16B*). This illustrated that the carbon input was the most influential parameter in the generic enzyme-based sugar model.

The Kinetic Model Predicted that Enzyme Flux Patterns Were Growth Dependent. To compare the enzyme flux patterns, two-dimension hierarchical clustering was performed on the fluxes together with the relative growth rate (RGR) (*SI Appendix, Table S3*). On the first dimension, ovaries were classified in three clusters related to the ovary growth status—namely, nongrowing unpollinated WT and anthesis (0 DAA) ovaries (cluster I), those growing 2 DAA (cluster II), and ovaries 4 DAA (pollinated WT and un- or pollinated *pro*, cluster III) (*SI Appendix, Fig. S17*). On the second dimension, clustering categorized variables in two main clusters related to metabolic activity with respect to the ovary growth status. For instance, ovaries that were not growing or were in anthesis, were characterized by a low metabolic activity—i.e., low glycolysis (FBP-aldolase), low fluxes through kinases (FK, glucokinase [GK], phosphofructokinase [PFK]), and low sucrolytic activity (vacuolar acid invertase [Vac-Inv] and neutral invertase [Neu-Inv])—while high fluxes were through sucrose-phosphate synthase (SPS), resulting in a low hexose content and high Suc content (*SI Appendix, Fig. S11A*). By contrast, ovaries growing 4 DAA (cluster III), regardless of genotype, exhibited high metabolic activity—i.e., high glycolysis, high fluxes through kinases, and high sucrolytic activity while low SPS flux, which was associated with high hexose and low Suc contents. The ovaries growing 2 DAA exhibited an intermediate pattern with some variables being classified in the same cluster as those growing 4 DAA and those that were not growing or in anthesis (*SI Appendix, Fig. S17*). Overall, the clustering analysis of the measured and modeled metabolic data did not enable the separation of the WT and *pro* ovaries, on one side, and the pollinated and unpollinated *pro*, on the other. This strongly suggests that the metabolic rewiring that occurs during fruit setting is related more to ovary growth than to pollination or hormone status (Fig. 1).

Fruit Setting Shuts Down Suc Cycle and Induces Vacuolar Sugar Accumulation. The kinetic model predicted that fruit setting of the *pro* ovary, both pollinated and not, and that of the pollinated WT, were associated with an increase in Suc uptake that was linked to growth initiation (Fig. 5A). In this model, imported Suc was subsequently cleaved, mainly in the cytosol, by Neu-Inv and to some extent by SuSy. However, before fruit setting, even though Suc uptake flux was low, SPS flux was high, thus making the so-called Suc cycle highly active—i.e., about 80% of the cleaved Suc was resynthesized 0 DAA, regardless of the genotype. It is worth noting that fruit setting drastically shut down this cycle, mainly by decreasing the SPS flux, in such a way that only 10 to 20% of the cleaved Suc was resynthesized 4 DAA. Fluxes

of PFK—that catalyze the first step of glycolysis by the irreversible conversion of F6P to F1,6BP—were elevated, whereas those of the cytoplasmic fructose 1,6-bisphosphatase (FBPase)—that catalyzes the opposite direction of the carbon reaction through gluconeogenesis—were much lower in the fruit-setting ovaries (*SI Appendix, Fig. S17*). Thus, the FBP futile cycle was almost inactive (below 10%), regardless of the genotype and growth status (Fig. 5A).

Concomitantly, fruit setting induced a reallocation of Suc within the ovary cells. In nongrowing and anthesis ovaries, Suc, in contrast to Glc and Fru, was predicted to be predominantly localized to the cytosol (Fig. 5B), thus promoting the cytosolic Suc cycle, as described above. Between 2 and 4 DAA, the concentration of Suc decreased in the cytosol and that of Glc, Fru, and to a lesser extent Suc, increased in the vacuole. The increased levels of hexoses in the vacuole were correlated with the flux of Vac-Inv (Fig. 5A). Summarizing the contribution of these soluble sugars in each compartment, the cytosolic sugar concentration followed a mirror-shaped evolution pattern compared to the vacuolar concentrations. Indeed, whereas most of the sugars were accumulated, mainly as Suc, in the cytosol of the ovaries 0 and 2 DAA, most of the Suc and hexoses were localized to the vacuole in the growing ovaries 4 DAA (Fig. 5B). Overall, this sugar compartmentalization builds up an osmotic potential difference across the tonoplast of about 60 to 80 mOsm 4 DAA (calculated as the difference between the total sugar concentration in the vacuole minus that in the cytosol). The question was then raised as to what the mechanisms and regulations of this sugar reallocation upon fruit setting were.

Sugar Reallocation Is Concomitant with Tonoplast Carrier Induction.

The modeling approach considered the activity of two proton-coupled tonoplastic carriers, one specific to Suc and the other to both Fru and Glc (hexose), and enabled the calculation of sugar transport fluxes across the tonoplast at a steady state (Fig. 5C). Whereas the sugar exchanges between the vacuole and cytosol were small in nongrowing ovaries, upon fruit setting, Suc, and to a lesser extent Glc, were actively imported into the vacuole. In contrast, Fru transport remained extremely low, regardless of the ovary growth stage. However, a slight efflux, indicated by negative influx values, occurred from the vacuole 4 DAA in the growing ovaries. Fig. 5D presents time courses of the vacuolar carrier's activities, as predicted by the model. Upon fruit setting, the V_{\max} of both the Suc and hexose tonoplast carriers increased with time with each following a specific pattern, whereas the Suc carrier was up-regulated 2 and 4 DAA, and the hexose carrier was mainly up-regulated 4 DAA. The earlier up-regulation of the Suc carrier is possibly due to a high demand for Suc, for hexose production by Vac-Inv. In contrast, in nongrowing and anthesis ovaries, V_{\max} values of both the Suc and hexose tonoplast carriers were low and remained constant. The fact that similar profiles were noted for both the pollinated WT and *pro* and for the unpollinated *pro*, suggests that the underlying induction mechanisms may not be triggered by the pollination itself, but rather by growth initiation. Overall, these data suggest that tonoplast carriers are involved in the early metabolic events that cause sugars to accumulate in the vacuoles.

Vacuolar Sugar Accumulation Is Kinetically Controlled by Suc Transport.

To decipher the regulation of sugar accumulation in the vacuole during fruit setting, control coefficients were calculated according to the principles of metabolic control analysis (MCA) (37). Such a coefficient can determine how much (in terms of percentage) the vacuolar sugars would increase (positive sign) or decrease (negative sign) if a given parameter was increased by 1%. Most of the negative control was exerted by the

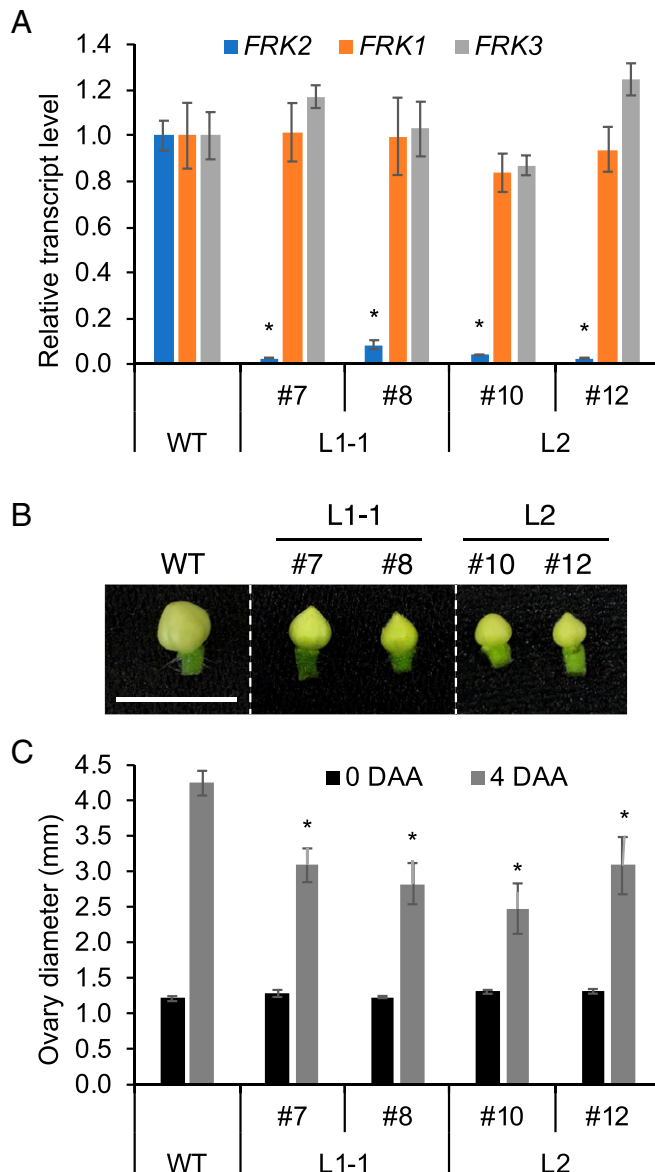


Fig. 6. Silencing of *FRK2* suppressed ovary growth during fruit set. (A) Expression analysis of three *FK* isozyme genes in the leaves of four individual plants (#7, #8, #10, and #12) derived from two independent transformed lines (L1-1 and L2). *CAC* gene was used as a reference and the expression levels of *FRK* genes were normalized to those of the WT. Values are mean \pm standard error of three independent leaves. (B) Representative pictures and (C) diameter of the ovaries at 4 DAA, which were pollinated at 0 DAA with WT pollen. Diameter of unpollinated ovaries at 0 DAA are also shown in C. Values in C are mean \pm standard errors of six replicates. (Scale bar in B, 1 cm.) Asterisks in A and C indicate significant differences from the corresponding WT (Student's *t* test, $P < 0.05$).

RGR on the vacuolar sugars, thus illustrating the dilution effect of growth on sugar storage (*SI Appendix, Fig. S18*). Crucially, although the flux in the Vac-Inv and V_{max} of the hexose carrier were both correlated with the hexose levels in the vacuole (Fig. 5A and D), neither the Vac-Inv nor the hexose carrier exerted any significant control (*SI Appendix, Fig. S18*). Most of the positive controls were shared between the fluxes of Suc uptake and the capacity of the vacuoles to transport it (Suc carrier V_{max}).

In nongrowing ovaries (unpollinated WT), the Suc carrier was the major controlling step. However, upon fruit setting, its control coefficient decreased for the pollinated WT and for the *pro*

(pollinated or not) ovaries, whereas the control exerted by the Suc uptake increased concomitantly (*SI Appendix, Fig. S18*). The Fig. 5D and *SI Appendix, Fig. S18* together, show that the lower control strength exerted by the vacuolar Suc carrier in the fruit-growing ovaries could be the consequence of the up-regulation of this carrier upon fruit setting. It is possible that the transcript abundances of the Suc carriers increased with fruit set, and this led to an increase in Suc entry into the vacuole, whereas saturated levels of transcripts or proteins of this carrier no longer acted as limiting factors for vacuolar sugar concentrations. Whether the transcript levels of some (putative) sugar carriers increased upon fruit setting was then considered. Despite the important role of the sugar carrier proteins on fruit set initiation, the transcript abundances of most of these genes did not exhibit good associations with fruit set (*SI Appendix, Fig. S19*), possibly

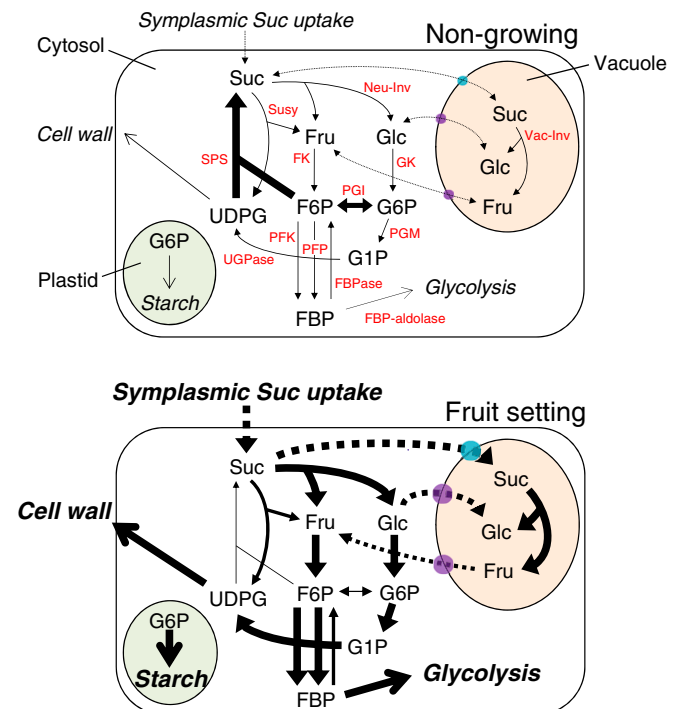


Fig. 7. Model-assisted overview of the metabolic and compartment shifts of carbohydrates during tomato fruit set, as controlled by pollination and PROCERA. A fruit set model was constructed from the data for the enzyme fluxes and metabolite levels that were kinetically calculated, as shown in Fig. 5. Suc and hexose carriers are indicated with sky blue- and purple-colored circles, respectively. The enzyme fluxes and tonoplastic activities are correlated with the size of their circles, while the levels of metabolite accumulation are correlated with the size of their letter. Vacuole and plastid compartments are highlighted by orange and green, respectively. Arrows indicate reactions, while dashed arrows indicate translocations between the cytosol and plastid or vacuole. In nongrowing ovaries (i.e., at anthesis and unpollinated WT), the Suc cycle, as indicated by the SPS and SuSy fluxes, was highly active, leading to relatively high Suc content in the ovary. In the fruit-growing ovaries, significant accumulations of starch were observed with increased fluxes of Suc uptake via the symplast, Neu-Inv, FK, and GK at 2 DAA. Such fluxes were further activated 4 DAA, where fluxes of Vac-Inv, PGM, UGPase, PFK, cell wall synthesis, and glycolysis were also activated. Output fluxes are italicized. Neu-Inv, neutral invertase; Vac-Inv, vacuolar acid invertase; SuSy, sucrose synthase; SPS, sucrose-phosphate synthase; FK, fructokinase; GK, glucokinase; PGI, phosphoglucosomerase; PGM, phosphoglycerate mutase; UGPase, UDP-glucose pyrophosphorylase; PFK, ATP phosphofructokinase; FBPase, fructose 1,6-bisphosphatase; Fru, fructose; Glc, glucose; Suc, sucrose; F6P, fructose-6-phosphate; G6P, glucose-6-phosphate; G1P, glucose-1-phosphate; UDPG, uracil-diphosphate glucose; FBP, fructose 1,6-bisphosphate.

because the transporter protein levels showed a relatively low correlation with the transcripts (*SI Appendix, Fig. S9*). However, in this framework, it is worth noting that such an adaptation of the carrier's capacity to satisfy metabolic needs, would make the growing ovaries more sensitive to the changes in the symplastic Suc availability. This model prediction is in line with the high fruit abortion levels that are usually observed when carbon availability is decreased (e.g., when tomato plants are grown in shaded conditions) (17).

Induction of Fructokinase Controls the Fru Concentration and Glc-to-Fru Ratio within the Cytosol. In plant cells, FK and GK activities are crucial for initiating cytosolic glycolysis by phosphorylating the hexoses that are either liberated by Neu-Inv or exported by the vacuole. To realistically model sugar metabolism, parametrization must consider the kinetic properties of FK and GK isozymes that are known to be specifically expressed in young tomato fruits (38, 39). Modeling the phosphorylation of Fru and Glu in a steady state showed that the FK and GK fluxes increased in parallel upon fruit setting (*SI Appendix, Fig. S20 A and B*), in correlation with the Suc uptake (Fig. 5A). However, the ratio between the FK and GK fluxes (~1.2 to 2.0, depending on the ovary stage; *SI Appendix, Fig. S20C*) emphasizes a pivotal role for FK in feeding the downstream catabolic (glycolysis) and anabolic (carbohydrate synthesis—i.e., cell wall components and starch) pathways. FK has been shown to be associated, together with invertase, with starch synthesis in pollen (40). Indeed, we observed remarkable starch accumulation in the plastids of fruit-growing ovaries, but not in the unpollinated WT ovaries (*SI Appendix, Fig. S11 A and C*), suggesting rapid and intense carbon fluxes into the starch synthesis, that are in line with the fact that Suc metabolism acts as a source of starch accumulation and vice versa (41). Overall, the flux through FK, in contrast to that of GK, was found to be correlated with its V_{\max} (*SI Appendix, Fig. S20D*), though only a few percentage points of the catalytic capacity (at most 10%) were readily used for metabolic activity (i.e., the flux-to- V_{\max} ratio for FK varied between 0.05 and 0.1, *SI Appendix, Fig. S20E*). These data suggest that the bursts of metabolic activity that occur upon fruit setting were, at least in part, triggered by the induction of FK. One of the metabolic markers of such a regulation is the elevated Glc-to-Fru ratio that was both measured and predicted in the growing versus non-growing ovaries (*SI Appendix, Figs. S11B and S21*).

The role of FK induction in this phenomenon has been further investigated by looking at the control coefficients exerted by this enzyme on the sugar concentrations and fluxes of enzymes and tonoplastic carriers. Regardless of the physiological state of the ovary, FK exerted a high level of control on the Glc-to-Fru ratio within the cytosol (*SI Appendix, Fig. S22A*), the cytosolic Fru concentrations, (*SI Appendix, Fig. S22B*), and, to some extent, the vacuolar Fru efflux via the Fru carrier (*SI Appendix, Fig. S22 B and C*). This suggests that the pivotal intermediate that is regulated by FK is the cytosolic Fru. This is in line with the fact that the affinity of FRK2 (the most abundant isozyme in tomato fruit-growing ovaries, *SI Appendix, Fig. S7A*) for Fru is usually very high, within the same range as the affinity of hexose kinases for Glc (39, 40).

To confirm the pivotal role of FK during fruit set, the *FRK2*-silenced lines were generated by an RNA interference (RNAi) approach. Two independent lines (L1-1 and L2) were selected in which the *FRK2* transcript level was significantly reduced compared to WT (although not for the other two isozymes, *FRK1* and *FRK3*) (Fig. 6A). Then, two sibling plants derived from each line were obtained. A total of four plants (#7 and #8 for L1-1, and #10 and #12 for L2) were used for the measurement of ovary growth upon pollination. Although ovary sizes of WT and

FRK2-silenced plants were equivalent at anthesis, the ovary size 4 DAA in the *FRK2*-silenced lines was significantly decreased by 27 to 42% when compared to the WT (Fig. 6 B and C). These results demonstrate the important role of *FRK2* in ovary growth during fruit set.

Discussion

Both Pollination-Dependent and -Independent Fruit Set Rewires the Central Metabolism Pathway with Increased GA Sensitivity. The primary purpose of this research was to identify the fundamental biochemical networks and regulations of fruit set, using multi-omics and kinetic modeling, and the GA hypersensitive mutant *pro*, as GA is believed to be the most epistatic hormone inducing fruit set (30). The integral analysis was able to define the transcripts, proteins, enzymes, and metabolites that were consistently impacted by both pollination and *pro*-induced parthenocarp and highlighted that the central metabolism was consistently rewired (Figs. 2 and 3 and *SI Appendix, Fig. S17*). High metabolic activity was evidenced by increased enzyme activities (*SI Appendix, Fig. S10*) and fluxes (*SI Appendix, Fig. S17*) in carbohydrate metabolism, glycolysis, and the TCA cycle, and by the up-regulation of the associated central metabolites, including hexoses, hexose phosphates, and organic and amino acids (Figs. 3 and 7 and *SI Appendix, Figs. S6 and S11*, and *Dataset S4*). In particular, the early responsive MetM3 module (*SI Appendix, Fig. S5*) contained the product of FK, F6P, whose levels were associated with FK activity and flux (Fig. 3 and *SI Appendix, Figs. S10 and S17*). Furthermore, FK activity was correlated with the protein abundances of the two isoforms (*FRK1* and *FRK2*), which were found in the MetM3-correlating transcript module GenM2 (Fig. 2, *SI Appendix, Fig. S7A* and Table S2, and *Dataset S3*), and with the corresponding transcript abundances (*SI Appendix, Fig. S7A*). These synchronous transcript, protein, enzyme, and metabolite fluctuations indicate tight and functional regulation of FK by the transcript levels, due to the initiation of fruit set, that was induced by GA signaling. Furthermore, FK showed a high catalytic capacity (*SI Appendix, Fig. S10*), that was also apparent from its low flux-to- V_{\max} ratio (*SI Appendix, Fig. S20*). Considering that high hexose phosphate levels coupled with low ATP-to-ADP ratios caused high fluxes in glycolysis (17), FK likely plays an important role in driving the metabolic rewiring that occurs in early phases of fruit setting (i.e., 2 DAA). Indeed, this study demonstrated that specific silencing of *FRK2* was associated with the suppression of ovary growth (Fig. 6). Notably, transgenic tomato plants in which three FK isoform genes (*FRK1*, *FRK2*, and *FRK3*) were simultaneously silenced, had reduced plant biomasses and increased flower abortion (42), and transgenic tomato plants in which cell wall invertase was enhanced, had improved fruit set efficiency associated with increased FK activity, under long-term, moderate heat-stress conditions (43). Taken together with the synchronous regulation as described above, we propose that FK is at least partially important for inducing fruit set as a driving force to feed the downstream pathways for biosynthesis of cell wall components and energy provision.

The WGCNA identified that MetM1 and MetM2, both of which correlated with GenM2 or GenM3 and peaked 4 DAA (SN-1), contained hexose and many derivatives and intermediates of the glycolysis and TCA cycles (Figs. 2 and 3, *SI Appendix, Fig. S5*, and *Dataset S4*). This suggests that fruit set shifts the emphasis to the cleavage of Suc by 4 DAA, rapidly providing an energy source and building blocks for the production of biomass, such as the components of the cell wall that are critical for rapid growth and the development of sink organs (fruit-setting ovaries) (Fig. 7) (24, 25). This metabolic activation most likely allows for the rapid increases of ovary biomass between 2 and 4 DAA

(Fig. 1C). Collectively, considering that bioactive GA levels also peaked 4 DAA and were correlated with ovary growth (Fig. 1 and *SI Appendix, Fig. S1*), it is suggested that levels of bioactive GAs or GA signaling pathways, determine sink capacities during fruit setting by transcriptionally elevating the subset of genes related to central metabolism (*SI Appendix, Fig. S7*).

Sugar Partitioning and Fluxes during Fruit Set. Fruit growth is highly dependent on carbon availability from the phloem's unloading of photosynthetic assimilates from source organs. In tomato, Suc unloading into the sink organ, followed by its degradation into hexoses, causes the generation of turgor pressure gradients between the sink and source organs, creating the osmotic potential for Suc unloading into the sink, and this is likely to be responsible for the degree of fruit growth (44). In this study, the kinetic model predicted the mode of sugar flux and the spatial and temporal distributions of sugars, as well as their metabolic regulation during fruit set (Figs. 5 and 7). In this model, Suc uptake into the ovary cytoplasm rapidly induced 2 DAA, and Suc was subsequently cleaved by the sugar interconversion enzymes Neu-Inv and SuSy (Fig. 5A). By 4 DAA, the resulting Glc and a large proportion of the unloaded Suc had been transported into the vacuoles via the tonoplast carrier proteins, where Vac-Inv produces hexose, which increases the total sugar content in the vacuoles (Figs. 5B and 7). Together with the organic acids (such as malate) or amino acids, this may decrease the osmotic potential of the vacuole, triggering water flow into this compartment and contributing to cell expansion via vacuole expansion. Large water flow across tonoplast likely occurs between 4 and 10 DAA in tomato fruits, until the vacuole volume fraction reaches its maximal value—e.g., about 80% of the cell volume (19).

It is of note that, in contrast to Glc, the resulting Fru is deposited within the cytosol and is most likely directly used by the FK for the generation of glycolytic fluxes. Outflux of the vacuolar Fru to the cytosol is likely due to the high demand of Fru by FK and results in a high Glc-to-Fru ratio in the vacuoles of growing ovaries (Fig. 5B and C and *SI Appendix, Fig. S21*). In contrast, the Suc biosynthesis through both Suc and FBP cycling appears to be nearly inactive in fruit-growing ovaries (Figs. 5A and 7). These observations suggest that Suc uptake by ovaries is highly dependent on phloem unloading and is maintained with the high fluxes of the temporal and spatial sugar partitioning, as well as the metabolic rewiring. In this context, the activation of metabolism during fruit setting is concomitant with the shutdown of the ATP-dissipating Suc cycle (45, 46), further indicating that energy production becomes a priority; this is consistent with the fact that the activities of the TCA cycle-related enzymes and metabolites were up-regulated in fruit-growing ovaries (Fig. 3 and *SI Appendix, Figs. S10 and S11*). The metabolic rewiring is most likely the key process of fruit set, which is in line with the evidence that the decline of the steady state of central metabolism impairs fruit set efficiency, or ovary growth (Fig. 6) (13, 14).

In summary, our results show that GA signaling induces a significant reprogramming of the central metabolism (i.e., metabolites in MetM1 to 3) via the expression of genes encoding pathway enzymes (i.e., genes in GenM1 to 3 and GenM7; Figs. 2–4 and *SI Appendix, Fig. S7*). Modeling Suc metabolism showed

that this reprogramming leads to a strong increase in Suc uptake by 2 DAA (Fig. 5A), followed on one hand by the reallocation of sugars to the vacuole by 4 DAA (Fig. 5B), leading to decreases in the osmotic potential within this compartment, promoting vacuole growth at the expense of the cytoplasm. However, on the other hand it leads to degradation that provides energy and building blocks for growth (Fig. 7). Fruit-setting ovaries thus shows high Suc metabolizing activities and maintain a low osmotic potential, while also maintaining a turgor pressure gradient against the source organs, which acts as a driving force for further phloem unloading. Therefore, GA-regulatory central metabolism most likely determines the sink capacity of fruit-setting ovaries. Such metabolic rewiring induced by the GA cascade is caused by depression of the PROCERA, at least in part through mediating the down-regulation of *SIHB15A*, a member of the negative module GenM1 (Figs. 2 and 4). Furthermore, the strong and early increase in FK capacity appeared as a key event counteracting sugar trapping in the vacuoles (Fig. 5 and *SI Appendix, Figs. S15, S18, and S20*), which appeared to be important for ovary growth during fruit set (Fig. 6).

The fact that GA sensitivity was already present in the *pro* mutant at anthesis indicates that a switch enabling fruit growth at this stage occurs upstream of the GA signaling. It will be interesting to investigate this switch in the future, for example, via mutagenesis of a genotype harboring the *pro* allele. Ultimately, a better understanding of fruit set metabolism will lead to new strategies for production, and in particular, the possibility of breeding for parthenocarpic fruits, and an increased control of fruit survival during the early stages of development.

Materials and Methods

Plant Materials, Growth Condition, and Experimental Procedures. This study used the tomato variety Micro-Tom WT and the *procera* (*pro*) mutant of the Micro-Tom. Both plant types were grown in a photoperiod of 16 h light at 25 °C (light)/20 °C (dark), under fluorescent lights at 300 $\mu\text{mol m}^{-2} \text{s}^{-1}$, with a nutrient solution (Ohtsuka house 1 and 2, OAT Agrio Co., Ltd) with an electrical conductivity (EC) of 1.6 dS m^{-1} . The genome edited *Slhb15a-ko*, the transgenic *FRK2-silenced* plants, and WT used for their comparison were also grown under the same condition as described above.

The details of the experimental procedures used for cytology, hormone profiling, transcriptome, proteome, metabolome, enzyme analysis, network analysis, vector construction, kinetic modeling analysis, MALDI-MSI, and qRT-PCR, are shown in *SI Appendix, SI Materials and Methods*.

Data Availability. Nucleotide sequence data have been deposited in DNA Data Bank of Japan (DDBJ) Sequence Read Archive ([DRA010267](https://www.ncbi.nlm.nih.gov/sra/DRA010267)). All study data are included in the article and supporting information.

ACKNOWLEDGMENTS. This work was supported by Grants-in-Aid for Scientific Research (KAKENHI), grants 15KK0273 and 221S0002; the Program to Disseminate Tenure Tracking System; the Japan Society for the Promotion of Science (JSPS) bilateral program to T.A.; and grants from the JSPS to Y. Shinozaki. (16J00582 and 19K23672) and K.E. (16J00797). Y.G. and B.P.B. acknowledge Cédric Cassan for technical help and funding from PHENOME (ANR-11-INBS-012) and Fruit integrative modelling for a unified selection system (ANR-15-CE20-0009-01). We thank the National BioResource Project-Tomato for providing the tomato research material (TOMJPF0001). We also thank M. Okada, Y. Iida, Y. Fujimori, N. Inage, K. S. Miyamoto, R. Masuda, N. Ito, and K. Ito at the Gene Research Center and Y. Mitani at RIKEN for technical assistance.

1. S. Yamaguchi, Gibberellin metabolism and its regulation. *Annu. Rev. Plant Biol.* **59**, 225–251 (2008).
2. T. P. Sun, Gibberellin-GID1-DELLA: A pivotal regulatory module for plant growth and development. *Plant Physiol.* **154**, 567–570 (2010).
3. M. Ueguchi-Tanaka, M. Nakajima, A. Motoyuki, M. Matsuoka, Gibberellin receptor and its role in gibberellin signaling in plants. *Annu. Rev. Plant Biol.* **58**, 183–198 (2007).

4. G. W. Bassel, R. T. Mullen, J. D. Bewley, *procera* is a putative DELLA mutant in tomato (*Solanum lycopersicum*): Effects on the seed and vegetative plant. *J. Exp. Bot.* **59**, 585–593 (2008).
5. S. Livne *et al.*, Uncovering DELLA-independent gibberellin responses by characterizing new tomato *procera* mutants. *Plant Cell* **27**, 1579–1594 (2015).
6. M. de Jong, C. Mariani, W. H. Vriezen, The role of auxin and gibberellin in tomato fruit set. *J. Exp. Bot.* **60**, 1523–1532 (2009).

7. E. Carrera, O. Ruiz-Rivero, L. E. Peres, A. Atares, J. L. Garcia-Martinez, Characterization of the *procera* tomato mutant shows novel functions of the SIDELLA protein in the control of flower morphology, cell division and expansion, and the auxin-signaling pathway during fruit-set and development. *Plant Physiol.* **160**, 1581–1596 (2012).
8. C. Marti *et al.*, Silencing of DELLA induces facultative parthenocarp in tomato fruits. *Plant J.* **52**, 865–876 (2007).
9. J. Hu, A. Israeli, N. Ori, T. P. Sun, The interaction between DELLA and ARF/IAA mediates crosstalk between gibberellin and auxin signaling to control fruit initiation in tomato. *Plant Cell* **30**, 1710–1728 (2018).
10. J. C. Serrani, O. Ruiz-Rivero, M. Fos, J. L. Garcia-Martinez, Auxin-induced fruit-set in tomato is mediated in part by gibberellins. *Plant J.* **56**, 922–934 (2008).
11. W. H. Vriezen, R. Feron, F. Maretti, J. Keijman, C. Mariani, Changes in tomato ovary transcriptome demonstrate complex hormonal regulation of fruit set. *New Phytol.* **177**, 60–76 (2008).
12. H. Wang *et al.*, Regulatory features underlying pollination-dependent and -independent tomato fruit set revealed by transcript and primary metabolite profiling. *Plant Cell* **21**, 1428–1452 (2009).
13. M. A. D'Aoust, S. Yelle, B. Nguyen-Quoc, Antisense inhibition of tomato fruit sucrose synthase decreases fruit setting and the sucrose unloading capacity of young fruit. *Plant Cell* **11**, 2407–2418 (1999).
14. M. I. Zanon *et al.*, RNA interference of LIN5 in tomato confirms its role in controlling Brix content, uncovers the influence of sugars on the levels of fruit hormones, and demonstrates the importance of sucrose cleavage for normal fruit development and fertility. *Plant Physiol.* **150**, 1204–1218 (2009).
15. M. Fos *et al.*, Polyamine metabolism is altered in unpollinated parthenocarpic *pat-2* tomato ovaries. *Plant Physiol.* **131**, 359–366 (2003).
16. S. Osorio *et al.*, Systems biology of tomato fruit development: Combined transcript, protein, and metabolite analysis of tomato transcription factor (*nor*, *rin*) and ethylene receptor (*Nr*) mutants reveals novel regulatory interactions. *Plant Physiol.* **157**, 405–425 (2011).
17. B. Biais *et al.*, Remarkable reproducibility of enzyme activity profiles in tomato fruits grown under contrasting environments provides a roadmap for studies of fruit metabolism. *Plant Physiol.* **164**, 1204–1221 (2014).
18. I. Belouah *et al.*, Modeling protein destiny in developing fruit. *Plant Physiol.* **180**, 1709–1724 (2019).
19. B. P. Beauvoit *et al.*, Model-assisted analysis of sugar metabolism throughout tomato fruit development reveals enzyme and carrier properties in relation to vacuole expansion. *Plant Cell* **26**, 3224–3242 (2014).
20. R. J. Pattison *et al.*, Comprehensive tissue-specific transcriptome analysis reveals distinct regulatory programs during early tomato fruit development. *Plant Physiol.* **168**, 1684–1701 (2015).
21. N. Olszewski, T. P. Sun, F. Gubler, Gibberellin signaling: Biosynthesis, catabolism, and response pathways. *Plant Cell* **14** (suppl.), S61–S80 (2002).
22. S. Liu *et al.*, Tomato AUXIN RESPONSE FACTOR 5 regulates fruit set and development via the mediation of auxin and gibberellin signaling. *Sci. Rep.* **8**, 2971 (2018).
23. M. de Jong, M. Wolters-Arts, R. Feron, C. Mariani, W. H. Vriezen, The *Solanum lycopersicum* auxin response factor 7 (*SlARF7*) regulates auxin signaling during tomato fruit set and development. *Plant J.* **57**, 160–170 (2009).
24. P. Langfelder, S. Horvath, WGCNA: An R package for weighted correlation network analysis. *BMC Bioinformatics* **9**, 559 (2008).
25. T. Tohge, M. Watanabe, R. Hoefgen, A. R. Fernie, Shikimate and phenylalanine biosynthesis in the green lineage. *Front. Plant Sci.* **4**, 62 (2013).
26. A. R. Fernie, F. Carrari, L. J. Sweetlove, Respiratory metabolism: Glycolysis, the TCA cycle and mitochondrial electron transport. *Curr. Opin. Plant Biol.* **7**, 254–261 (2004).
27. K. Kang, Y. S. Kim, S. Park, K. Back, Senescence-induced serotonin biosynthesis and its role in delaying senescence in rice leaves. *Plant Physiol.* **150**, 1380–1393 (2009).
28. L. Li *et al.*, Comprehensive investigation of tobacco leaves during natural early senescence via multi-platform metabolomics analyses. *Sci. Rep.* **6**, 37976 (2016).
29. M. Watanabe *et al.*, Comprehensive dissection of spatiotemporal metabolic shifts in primary, secondary, and lipid metabolism during developmental senescence in Arabidopsis. *Plant Physiol.* **162**, 1290–1310 (2013).
30. Y. Shinozaki *et al.*, Ethylene suppresses tomato (*Solanum lycopersicum*) fruit set through modification of gibberellin metabolism. *Plant J.* **83**, 237–251 (2015).
31. Y. Shinozaki, H. Ezura, T. Ariizumi, The role of ethylene in the regulation of ovary senescence and fruit set in tomato (*Solanum lycopersicum*). *Plant Signal. Behav.* **13**, e1146844 (2018).
32. K. A. Green, M. J. Prigge, R. B. Katzman, S. E. Clark, CORONA, a member of the class III homeodomain leucine zipper gene family in Arabidopsis, regulates stem cell specification and organogenesis. *Plant Cell* **17**, 691–704 (2005).
33. Q. Xu *et al.*, Domain-specific expression of meristematic genes is defined by the LITTLE ZIPPER protein DTM in tomato. *Commun. Biol.* **2**, 134 (2019).
34. Z. Shimatani *et al.*, Targeted base editing in rice and tomato using a CRISPR-Cas9 cytidine deaminase fusion. *Nat. Biotechnol.* **35**, 441–443 (2017).
35. O. Thimm *et al.*, MAPMAN: a user-driven tool to display genomics data sets onto diagrams of metabolic pathways and other biological processes. *Plant J* **37**, 914–939 (2004).
36. S. Damon, J. Hewitt, M. Nieder, A. B. Bennett, Sink metabolism in tomato fruit: II. Phloem unloading and sugar uptake. *Plant Physiol.* **87**, 731–736 (1988).
37. S. Schuster, R. Heinrich, The definitions of metabolic control analysis revisited. *Bio-systems* **27**, 1–15 (1992).
38. E. Claeysen, J. Rivoal, Isozymes of plant hexokinase: Occurrence, properties and functions. *Phytochemistry* **68**, 709–731 (2007).
39. Y. Kanayama *et al.*, Tomato fructokinases exhibit differential expression and substrate regulation. *Plant Physiol.* **117**, 85–90 (1998).
40. D. Granot, R. David-Schwartz, G. Kelly, Hexose kinases and their role in sugar-sensing and plant development. *Front. Plant Sci.* **4**, 44 (2013).
41. S. Streb, S. C. Zeeman, Starch metabolism in Arabidopsis. *Arabidopsis Book* **10**, e0160 (2012).
42. O. Stein *et al.*, The tomato plastidic fructokinase *SIFRK3* plays a role in xylem development. *New Phytol.* **209**, 1484–1495 (2016).
43. Y. H. Liu, C. E. Offler, Y. L. Ruan, Cell wall invertase promotes fruit set under heat stress by suppressing ROS-independent cell death. *Plant Physiol.* **172**, 163–180 (2016).
44. S. Osorio, Y. L. Ruan, A. R. Fernie, An update on source-to-sink carbon partitioning in tomato. *Front. Plant Sci.* **5**, 516 (2014).
45. B. Nguyen-Quoc, C. H. Foyer, A role for “futile cycles” involving invertase and sucrose synthase in sucrose metabolism of tomato fruit. *J. Exp. Bot.* **52**, 881–889 (2001).
46. J. S. Amthor *et al.*, Engineering strategies to boost crop productivity by cutting respiratory carbon loss. *Plant Cell* **31**, 297–314 (2019).